Title

Impact of Maximal Overexpression of a Non-toxic Protein on Yeast Cell Physiology

Authors

Yuri Fujita[1], Shotaro Namba[1], Hisao Moriya[2]

Affiliations

[1]Graduate School of Environmental, Life, Natural Science and Technology, Okayama University

[2]Faculty of Environmental, Life, Natural Science and Technology, Okayama University

Competing interests

The authors declare that there are no competing interests.

Author contribution

YF and HM conceived and designed the experiments, YF performed experiments, YF, SN, and HM analyzed the data, and YF and HM wrote the paper.

Summary

While it is recognized that excess expression of non-essential proteins burdens cell growth, the physiological state of cells under such stress is largely unknown. This is because it is challenging to distinguish between adverse effects arising from the properties of the expressed excess protein (cytotoxicity) and those caused solely by protein overexpression. In this study, we attempted to identify the model protein with the lowest cytotoxicity in yeast cells by introducing a new neutrality index. We found that a non-fluorescent fluorescent protein (mox-YG) and an inactive glycolytic enzyme (Gpm1-CCmut) showed the lowest cytotoxicity. These proteins can be expressed at levels exceeding 40% of total protein while maintaining yeast growth. The transcriptome of cells expressing mox-YG to the limit indicated that the cells were in a nitrogen source requirement state. Proteome analysis revealed increased mitochondrial function and decreased ribosome abundance, like the inactivated state of the TORC1 pathway. The decrease in ribosome abundance was presumably due to defective nucleolus formation, partially rescued by a mutation in the nuclear exosome. These findings suggest that massive overexpression of excess protein, termed protein burden, causes nitrogen source starvation, a metabolic shift toward more energy-efficient respiration, and a ribosomal biosynthesis defect due to an imbalance between ribosomal protein and rRNA synthesis in the nucleolus.

Introduction

Expression levels of proteins are optimized to maximize the fitness of organisms, and the evolutionary principle that determines those levels is considered to be demand and constraint (Bruggeman et al., 2020) (**Figure 1A**). Demand is the evolutionary pressure that works to increase the expression of a protein to meet the requirements of its function, and constraint is the evolutionary pressure that works to decrease the expression of a protein to avoid the negative effects produced by excess protein. Constraints appear as disturbances in cellular function when the protein is overexpressed (**Figure 1A**, the red arrow). The mechanisms of constraining expression levels, or defects due to overexpression, can be roughly classified into four major categories (Moriya, 2015) (**Figure 1B**). "Resource overload" (also called "burden") (Kastberg et al., 2022) is a disorder in which intracellular resources used for protein processing, such as synthesis, localization, degradation, and modification of proteins, are depleted or monopolized by the processing of that protein, resulting in a disruption of processing of other proteins (Dong et al., 1995; Eguchi et al., 2018; Kintaka et al., 2020, 2016); (Stoebel et al., 2008). This phenomenon occurs in proteins with high expression levels. "Stoichiometry imbalance" is a disorder triggered by an imbalance of amounts between constituents within complexes, leading to untimely activation or inactivation (pathway modulation), degradation (resource overload), aggregation (promiscuous interactions), etc. (Kaizu et al., 2010; Makanae et al., 2013; Papp et al., 2003). This occurs due to the overexpression of proteins that form complexes. "Pathway modulation" is a disorder in which pathways are untimely activated or inactivated. This occurs especially with overexpression of proteins involved in pathway regulation, such as metabolic enzymes, kinases and phosphatases, and transcription factors (Prelich, 2012; Youn et al., 2017). "Promiscuous interaction" is a disorder in which weak interactions are enhanced by mass action to form complexes or aggregates that are not normally formed. This damages cellular function by inactivating essential proteins or overloading degradation resources, and is caused by overexpression of intrinsically disordered proteins or liquid-liquid phase-separating proteins (Bolognesi et al., 2016; Ma et al., 2010; Vavouri et al., 2009).

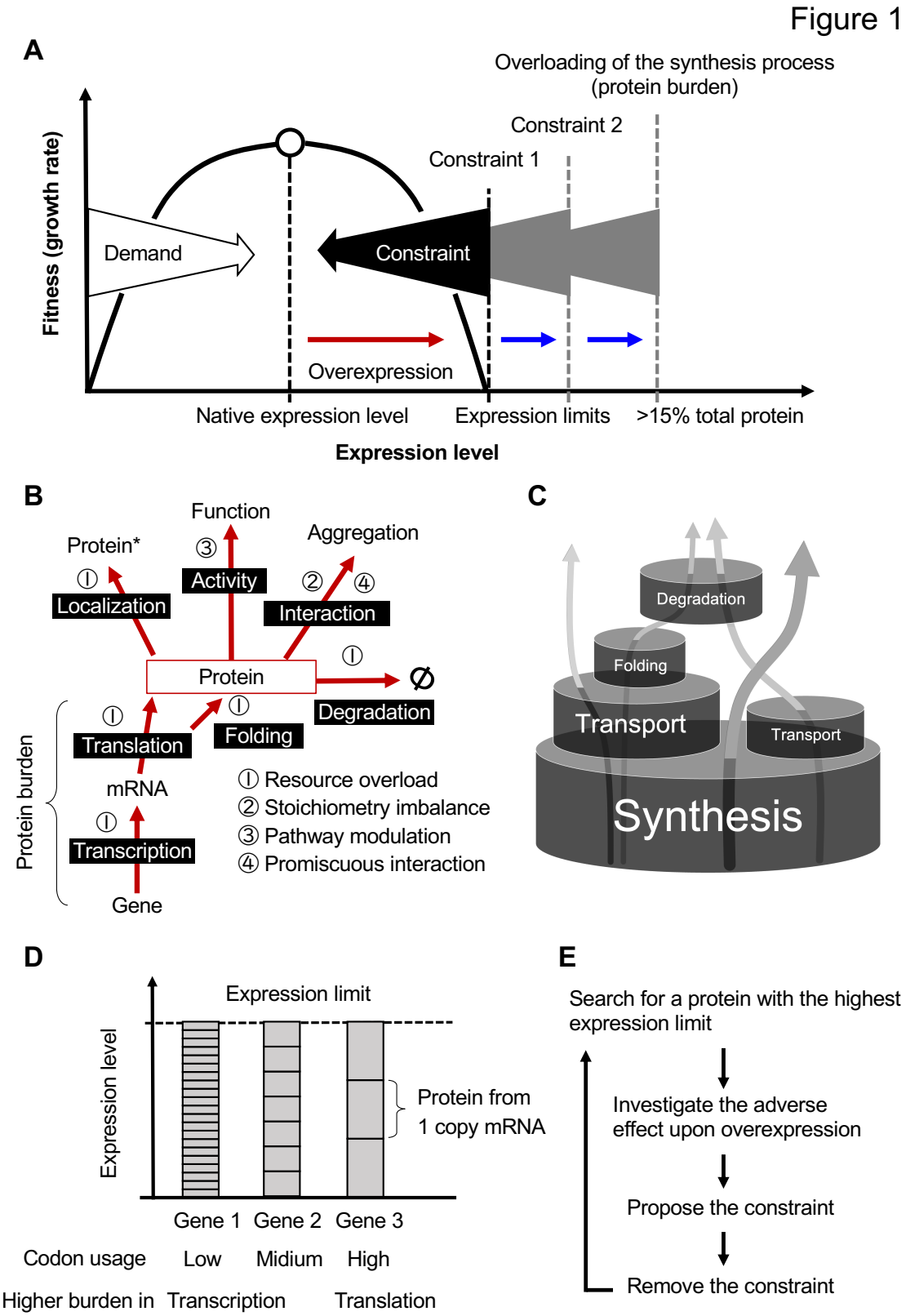

Figure 1. Schematic diagrams illustrating the constraints on protein expression levels. **A)** Protein expression levels are determined by demand and constraints (created by the authors, inspired by the work by Keren *et al.* (Keren et al., 2016). The existence of this evolutionary principle is revealed

63 by the relationship between fitness (growth rate) and expression level when the expression level is
64 altered, and in general, the native expression level provides the highest level of fitness for the organism
65 (Bruggeman et al., 2020). The existence of constraints is revealed by a decrease in fitness upon
66 overexpression (red arrow). Constraints determine the expression limit of the protein, i.e., the
67 expression level at which growth inhibition occurs (dotted lines), but there can be multiple constraints
68 for a single protein. The constraint that exists at the highest expression limit is protein burden.
69 **B)** Four major mechanisms that constrain protein expression levels. The figure outlines the fate of
70 proteins and shows what adverse effects occur upon overexpression (red arrows). The resource overload
71 that occurs within the synthesis process (transcription and translation) is specifically referred to as
72 protein burden. This diagram is a more concise redrawing of the author's earlier one (Moriya, 2015).
73 That asterisk means differentially localized proteins.
74 **C**) A barrel model for resource overload (modified from the author's earlier one) (Kintaka et al., 2020).
75 The size of the barrels represents the capacity of each process, and the arrows represent the fate of the
76 proteins processed there. The expression limit of a protein is defined by the lowest-capacity process
77 that processes the protein. Among these processes, synthesis, which processes all proteins, is considered
78 to have the largest capacity. Thus, proteins processed only by synthesis would have the highest
79 expression limits, and their overexpression would overload synthesis (i.e., cause protein burden).
80 Previous studies by the authors, conducted in this context, estimated that protein burden occurs at more
81 than 15% of total protein (Eguchi et al., 2018).
82 **D)** Difference in burden due to gene structure (codon optimization). The amount of transcription
83 required to achieve the same protein expression limit depends on the degree of codon optimization. This
84 may change whether transcription or translation results in a higher burden.
85 **E)** An ideal framework for protein burden studies. See text for details.

86

87

88 As the expression level of a protein increases, it eventually encounters one of the barriers created by
89 either these specified constraints or others that are unknown, all of which are related to the function and
90 physicochemical properties of the protein, and damage cellular function. The expression level at which

91 this occurs is referred to as the "expression limit" in this paper (see **Figure 1A**). If the constraints could
92 be removed from the protein, the expression limit would increase. For example, if components of a
93 complex are simultaneously expressed to resolve a stoichiometry imbalance, the expression limits of
94 those proteins will be increased (Kaizu et al., 2010; Makanae et al., 2013). In this manner, when (one)
95 constraint is removed from a protein, the expression limit would increase until the next constraint barrier
96 is hit (**Figure 1A**, dotted lines). The amount of expression limit created by a constraint barrier depends
97 on the type of constraint. Stoichiometry imbalances, pathway modulations, and promiscuous
98 interactions would create different expression limits for each protein. This is because they are
99 determined by the activity, regulatory mechanism, and physicochemical properties of each protein. On
100 the other hand, resource overload is presumed to be determined to some extent by the capacities of the
101 processes in the cell (Kintaka et al., 2020) (**Figure 1C**). Essentially, the synthesis, in which all proteins
102 are processed, should have the largest capacity, while processes such as transport, folding, and
103 degradation, in which only a fraction of proteins are processed, should have smaller capacities. In fact,
104 adding transport or degradation signals to a cytosolic protein lowers the expression limit (Kintaka et al.,
105 2016). In that light, the final constraint barrier that emerges when all possible constraints are removed
106 is the overloading of the synthesis process.
107
108 Overloading of the synthesis process is specifically referred to as "protein burden" or "protein cost"
109 (Eguchi et al., 2018; Kafri et al., 2016). It has long been the subject of study, mainly as an effect on
110 growth produced by excess (gratuitous) proteins that are not necessary for cellular function (Bruggeman
111 et al., 2020; Scott et al., 2010). This idea was first proposed in studies of the cost of unnecessary
112 induction of the *lac* operon in *Escherichia coli* (Koch, 1983). In recent years, much attention has been
113 paid to the actual mechanisms by which massive expression of excess protein inhibits growth and the
114 response of cells (Farkas et al., 2018; Kafri et al., 2016; Metzl-Raz et al., 2020). During protein burden,
115 it is presumed that depletion of the materials, machinery, and factors necessary for transcription and
116 translation occurs, along with competition from these monopolies. In particular, amino acids and
117 aminoacyl-tRNAs are major candidates for depletion (Kastberg et al., 2022). In addition, ribosomes,
118 which are crucial for protein synthesis, themselves require significant resources for their synthesis and

119 have therefore been considered major candidates for depletion during protein burden, as they compete
120 for these limited resources (Metzl-Raz et al., 2017). Mechanistic analysis of protein burden in budding
121 yeast, a model eukaryotic cell, has been intensively conducted by Barkai and colleagues, who reported
122 that transcription is rate-limiting in phosphate starvation and translation in nitrogen source starvation
123 (Kafri et al., 2016), and that basic transcription factors are limiting resources (Metzl-Raz et al., 2020).
124 In addition, a cellular response in the form of increased cell size and enhanced protein synthesis capacity
125 has been observed (Kafri et al., 2016). Thus, the previously expected decrease in ribosomes has not
126 been detected.
127
128 As mentioned above, to investigate protein burden, we need to overexpress proteins with minimal
129 constraints. This is because overexpressing proteins with additional constraints cannot overload the
130 synthetic process, as the additional constraints reduce the expression limits (**Figure 1A**). Also, the
131 cellular damage and cellular response generated by the constraint mask the protein burden response.
132 However, it remains unclear which proteins are not subject to constraints other than protein burden.
133 Proteins that would induce protein burden have been determined by assuming that they would be
134 minimally constrained based on their properties, and this assumption has been confirmed
135 experimentally. Model proteins selected in this manner in yeast include fluorescent proteins (FPs) and
136 certain glycolytic enzymes (Eguchi et al., 2018; Farkas et al., 2018; Kafri et al., 2016; Kintaka et al.,
137 2020, 2016). FPs do not have a specific function or interaction partner in yeast cells and are not localized.
138 On the other hand, glycolytic enzymes are naturally expressed at very high levels and are thus
139 considered to be less constrained. Notably, these proteins exhibit an expression limit of approximately
140 15% of total protein in yeast cells (Eguchi et al., 2018; Kintaka et al., 2016). However, it is not clear
141 whether these proteins are free from constraints other than protein burden. This is because there may
142 be unknown constraints, and there is no evidence that the measured expression limit is the "true limit"
143 at which protein burden occurs.
144
145 In addition to the protein (amino acid sequence) itself, there is another aspect to be considered when
146 selecting a model for protein burden. That is the nucleotide sequence of the gene used for expression,

147 i.e., transcriptional, and translational regulatory sequences, codon usage, and so on (**Figure 1D**). For
148 example, if a protein is to be expressed to the limit by a less codon-optimized and thus less
149 translationally efficient mRNA, a large amount of mRNA would be required, which would induce a
150 greater burden on transcription. Conversely, a similar attempt by an mRNA with high translation
151 efficiency would induce a greater burden on translation. These are the constraints inherent in protein
152 synthesis itself. Although there is some evidence that protein synthesis in nature is economically
153 designed to optimally load transcription and translation (Frumkin et al., 2017; Hausser et al., 2019;
154 Mahima and Sharma, 2023), it still needs to be determined what the genetic design should be to
155 minimize the burden.
156
157 Considering the above circumstance, a realistic approach to protein burden requires more than just
158 drawing straightforward conclusions from the overexpression of a single model protein (or gene).
159 Rather, it requires experimentally identifying proteins with the highest possible expression limits,
160 investigating the negative impacts of their overexpression, and, if any constraints are revealed,
161 examining whether their removal can increase expression limits. Through successive iterations, this
162 process gradually deepens our understanding of protein burden (**Figure 1E**). In each iteration, the least
163 constrained protein (and its gene) will be generated and utilized as a benchmark for further investigation
164 into proteins with high (or low) expression limits and the adverse effects of their overexpression. This
165 will (unintentionally) elucidate a new mechanism of constraint. Indeed, the enhanced green fluorescent
166 protein (EGFP), which we have used as a model for protein burden (Kintaka et al., 2020, 2016; Makanae
167 et al., 2013), was found to form a chaperone-entrapped aggregate upon overexpression and trigger the
168 heat shock response due to its low folding ability (Namba et al., 2022). Its overexpression also causes
169 abnormal yeast cell morphology through proteasomal stress as it contains cysteines. The moxGFP
170 (mox), which improved folding properties and lacks cysteine residues (Costantini et al., 2015), showed
171 a higher expression limit and no longer induced abnormal morphologies. However, even when
172 overexpressing mox, the anticipated depletion and competition for factors, or cellular responses to them
173 have not been observed (Namba et al., 2022).
174

175 In this study, we found that a mutation causing loss of fluorescence in mox, and other fluorescent
176 proteins increased the expression limit up to 3-fold, to more than 40% of total protein. Introducing a
177 neutrality index (NI) to assess protein constraint, we found that non-fluorescent mox (mox-YG) and
178 enzymatically inactive Gpm1 (Gpm1-CCmut) are currently the least constrained. Upon overexpression
179 of mox-YG, depletion of amino acid or nitrogen sources, decreased ribosomal expression, and a
180 metabolic shift from glycolysis to oxygen respiration were observed. Thus, physiological states, as
181 anticipated with such protein burdens, are only generated by massive overexpression of proteins with
182 significantly lower constraints. Some of the responses found appear to be due to inactivation of the
183 TORC1 pathway, suggesting that eukaryotic cells use this regulatory pathway to buffer protein burden.
184 In the burdened cells, the nucleolus was dysplastic, and mutations in the nuclear exosome partially
185 restored this. Thus, the abnormal formation of liquid-liquid phase-separated organelles due to dilution
186 may be one of the defects caused by the strong protein burden.

187 # Results

188 **Fluorescent property is a constraint on the expression of fluorescent proteins.**

189 To evaluate the expression limits of FPs, we overexpressed FPs to levels that induced growth inhibition.
190 Gene constructs, in which the *TDH3* promoter controls the target protein genes, were incorporated into
191 plasmids designed for the genetic-tug-of-war (gTOW) method (**Figures 2A, 2_S1A**) (Moriya et al.,
192 2006). Subsequently, yeast cells were transformed and cultured in a medium depleted of leucine. The
193 maximum growth rate (MGR) of cells was calculated from serial measurements of optical density at
194 660 nm (OD_{660}). Protein levels were determined through the analysis of proteins from cells in the
195 logarithmic growth phase (**Figure 2_S1B**). For each protein, we also analyzed a mutant in which the
196 Tyr residue forming the fluorophore was replaced with Gly (YG mutation), resulting in a loss of
197 fluorescence. This is because we unexpectedly found that this mutation substantially increased the
198 expression limits of FPs (see below).

199

200 Overexpression of the FPs and mutants all caused growth inhibition (**Figure 2B, C**). EGFP and mox
201 were expressed at about 15% of the total protein as previously reported (Kintaka et al., 2016), but
202 mCherry (mChe) and YG mutants were expressed at higher levels. Mox-YG expressed 44% of the total
203 protein (**Figures 2D, E)**. Our previous work had evaluated only expression limits (Eguchi et al., 2018),
204 but we realized that we could not properly assess the constraints on each protein if the growth rates at
205 the expression limit were different. For example, the mChe's expression limit (20%) is higher than that
206 of sfGFP (17%), but the relative MGRs are 20% and 80%, respectively, which is much lower for mChe.
207 The relationship between %MGR and %protein level when the vector is set at 100% is shown in the
208 scatter plot in **Figure 2F**. The lower left indicates more constraint as lower expression levels lead to
209 growth inhibition, and the upper right indicates less constraint as higher expression levels do not cause
210 growth inhibition. Here, we describe “unconstrained” as “neutral” and calculate the neutrality index
211 (NI) as the product of %MGR and %protein level.

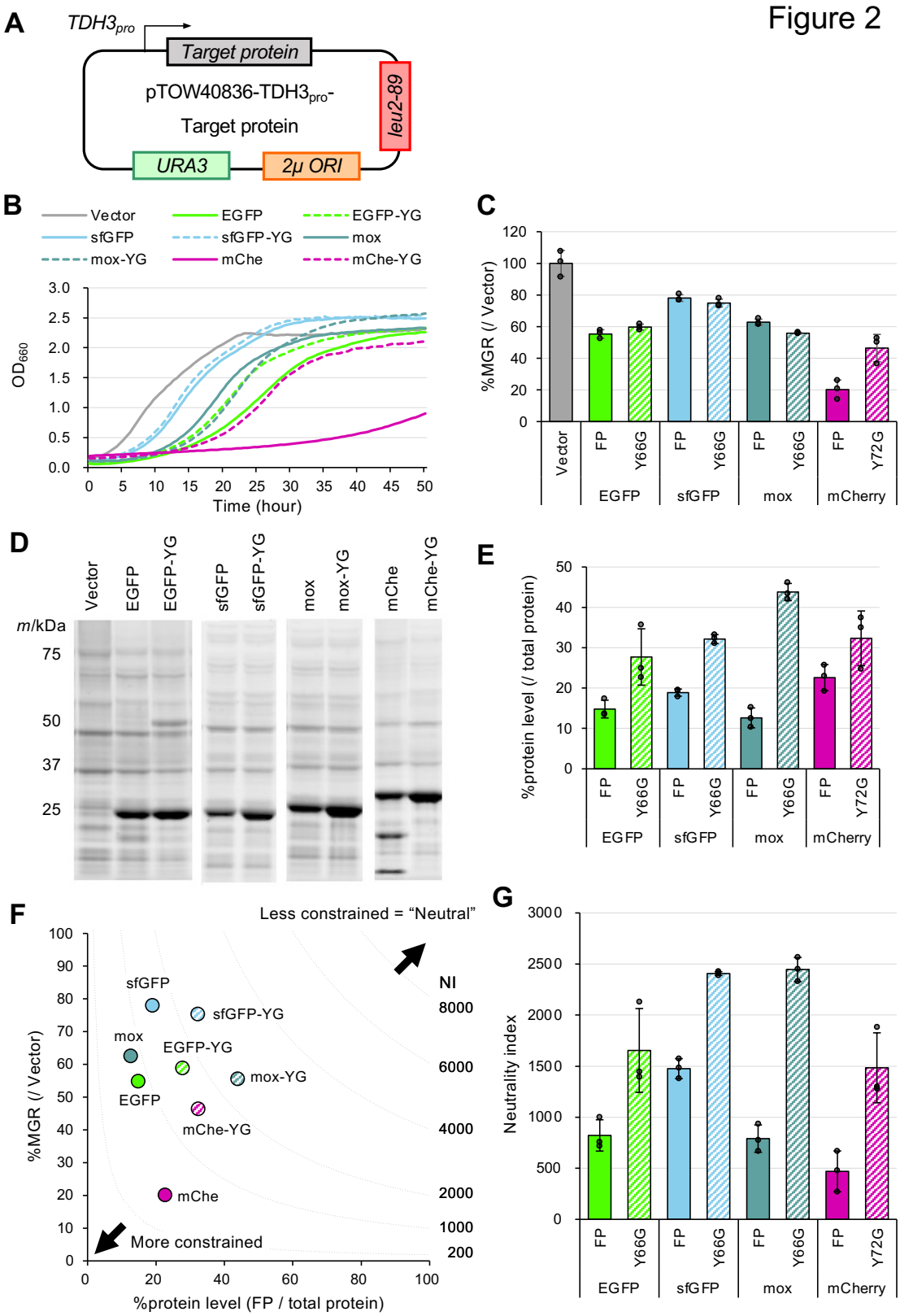

212

213 **Figure 2. Evaluation of expression constraint (or neutrality) of fluorescent proteins.**

214 **A**) Experimental setup of the analysis. Target proteins were expressed under the control of the *TDH3*
215 promoter ($TDH3_{pro}$) using the multicopy plasmid pTOW40836. The cells were pre-cultured under –Ura
216 conditions, and then cultured in –LeuUra conditions.
217 **B**) Growth curves of the vector control and cells overexpressing FPs and their mutants in synthetic
218 medium (–LeuUra). The solid or dotted lines show the average calculated from three biological
219 replicates. Growth curves with the standard deviations (SD) of replicates are shown in **Figure 2_S2**.
220 **C**) MGR of cells overexpressing FPs and their mutants (percent over the vector control).
221 **D**) Gel images of SDS-PAGE-separated proteins extracted from cells overexpressing FPs. All proteins
222 were separated after staining with a fluorescent dye.
223 **E**) Protein level of the target protein (percent over the total protein). The amount was calculated from
224 the intensity of the target bands separated by SDS-PAGE of **D**. See **Figure 2_S1B** for the method of
225 FP and total protein quantification. Note that EGFP-YG and mCherry may not be accurately measured
226 due to dimerization and cleavage of the protein, respectively.
227 **F**) Relationship between MGR and the protein level. MGR data are the same as in **C**, and the protein
228 level data are the same as in **E**. The neutrality indexes (NIs), calculated from the products of MGR and
229 protein levels, are indicated by the lines. If the investigated proteins have the same NI, they are located
230 on the same dotted line segment.
231 **G**) The neutrality index for the FPs and mutants. The neutrality index is the product of %MGR (/vector)
232 and %protein level (/total protein).
233 The bars and error bars in **C**, **E**, and **G** show the means and SDs calculated from three biological
234 replicates. The raw data is shown with dot plots.
235
236
237 Note that the regime of NI in **Figure 2F** shows a theoretical neutrality distribution but does not show
238 the relationship between growth rate and the expression level when the expression level of a protein
239 with a particular neutrality is increased or decreased. For example, 20% of the growth rate would be
240 maintained when the expression of mox-YG (NI = 2,400) is increased to 100%, but this is not realistic.
241

242 The NI of each protein indicates that introducing a non-fluorescent mutation in FPs uniformly increases
243 neutrality (**Figure 2G**), suggesting that "having fluorescence" is a constraint on the expression of FPs.
244 The most neutral proteins were sfGFP-YG and mox-YG, with NIs of about 2,400. Notably, despite
245 significant differences in the degree of growth inhibition and expression limits between the two proteins,
246 their NIs are nearly identical (**Figures 2F, G**). They differ only in two amino acid residues (Cys - Ser)
247 (**Figure 2_S3**), which seem to generate differences in expression efficiency. However, this does not
248 appear to affect their NIs.
249
250 We also investigated the impact of expression efficiency on NI with another FP, mChe. The mChe used
251 in this study is codon optimized (the codon adaptation index (CAI) = 0.584) (Keppler-Ross et al., 2008),
252 while the mChe used by Kafri *et al.* for protein cost analysis (here referred to as mChe-Kafri) is not
253 codon optimized (CAI = 0.236) (Kafri et al., 2016). When overexpressed, mChe-Kafri (and mChe-
254 Kafri-YG) had lower expression and growth inhibition than mChe (and mChe-YG) (**Figures 2_S4A-**
255 **D**). This may be due to the lower translation rate of mChe-Kafri mRNA. However, their NIs were not
256 significantly different, especially for the YG mutation (**Figures 2_S4E, F**). Thus, the constraints
257 indicated by NI are apparently not affected by translation efficiency. In the study using this mCherry-
258 Kafri, it was also reported that the more mChe-Kafri was expressed, the more the cells enlarged (Kafri
259 et al., 2016). However, no cell enlargement was observed with mox-YG, which can be expressed more
260 than mCherry. Interestingly, the mChe-YG cells did not show enlargement (**Figures 2_S5A, B**),
261 indicating that cell enlargement is a phenomenon that occurs specifically when fluorescent mChe is
262 overexpressed.
263
264 It should be noted that the growth inhibition caused by the overexpression of mox-YG in this study is a
265 burden on translation rather than on transcription. This is because overexpression of a frameshift mutant,
266 in which four nucleotides were inserted directly after the ATG of the mox-YG gene, abolished the
267 notable growth delay (**Figures 2_S5C, D**).
268
269 **Constraint on fluorescent protein expression arises from fluorophore properties.**

270 Next, we further analyzed the possibility that fluorescence constrains the expression of FPs. When yeast
271 was grown in the dark, the degree of growth inhibition of mox was the same (**Figure 2_S6A**) and the
272 expression limit of mox was rather increased (**Figure 2_S6B**). Phototoxicity does indeed exist when
273 expressing mox with fluorescence. This is because, when exposed to strong light, cells overexpressing
274 mox show a reduced growth rate **(Figure 2_S6C-E**) and abnormalities in their internal structures
275 (**Figure 2_S6F**). However, the expression limits of mox and mox-YG were almost unchanged by the
276 light (**Figure S2_S6G, H**). Thus, the constraint was not due to phototoxicity itself.
277
278 The number of Tyr residues was also irrelevant because NI was like that of mox-YG when a single Tyr
279 was added to the C-terminus of mox-YG (**Figure 2_S7C-E**). Reactive oxygen species (H_2O_2) are
280 generated during fluorophore formation. When H_2O_2 was added to the medium, stronger growth
281 inhibition occurred only in mox (**Figure 2_S7F-H**). This suggests that the reactive oxygen species
282 generated during fluorophore formation are responsible for the constraint. However, this possibility is
283 not supported by the omics analysis described later (see Discussion). Mox-YG, like mox, was present
284 throughout the cytoplasm and did not cause any characteristic localization or aggregation (**Figure 2_S8**).
285
286 During this study, we examined a moxGFP (mox-T203I) in which Thr203 was accidentally replaced by
287 Ile (**Figure 2_S9**). The fluorescence of this mutant is reduced to 78% of mox (**Figures 2_S9A-C**). The
288 growth rate of the cells expressing this mox-T203I was like that of mox and mox-YG (**Figure 2_S9E**).
289 Still, the expression limit was intermediate between mox and mox-YG (**Figure 2_S9F**), resulting in the
290 NI intermediate between mox and mox-YG (**Figure 2_S9G**). This result further supports that
291 fluorescence is related to constraints. However, as mentioned above, fluorescence emission itself should
292 not be toxic (**Figure 2_S6**). We next focused on the formation process of the fluorophore: the tyrosine
293 of the GFP fluorophore undergoes phenol and phenolate state changes, with Thr203 stabilizing the
294 phenol form and substitution to Ile reducing the phenolate form (Kummer et al., 2000). Furthermore, in
295 enhanced GFPs such as mox, substitution of Ser65 before Tyr66 for Thr anchors the phenolate form.
296 To investigate the possibility that this is a factor determining the limit of mox, we produced mox with
297 Thr65 replaced with Ser and examined its expression limit. The mox-T65S mutant was expressed 12%

298 more than mox (**Figures 2_S9H, I**), suggesting that the phenol-type fluorophore can be a limiting factor
299 for the expression level of the fluorescent protein, while the concrete mechanism is still unclear.
300
301 **The activities of the glycolytic enzymes Gpm1 and Tdh3 may constrain their expression.**
302 We previously investigated the expression limits of a group of glycolytic enzymes in *S. cerevisiae*, with
303 Gpm1 and its catalytic center (CC-) mutant having the highest expression limits (Eguchi et al., 2018).
304 Here, we evaluated the neutrality of the wild types and their CC-mutants of Tdh3 and Gpm1 (**Figure**
305 **3**). The growth rates at the expression limits were higher in the CC-mutant for both Tdh3 and Gpm1,
306 and in Gpm1, the CC-mutant grew two-fold faster (**Figures 3A, B**, **3_S1**). The protein levels of wild
307 types and mutants of both proteins were not significantly different (**Figures 3C, D**). The calculated NIs
308 were highest for Gpm1 CC-mutant, which was equivalent to that of mox-YG (**Figures 3E, F**). Thus,
309 mox-YG and Gpm1 CC-mutant are the least constrained proteins to this point. We previously concluded
310 that the activities of glycolytic enzymes generally do not affect their expression limits (Eguchi 2018),
311 but their neutralities suggest that their activities can become constraints in some way. This may be due
312 to a disturbance in metabolism or a property of the active enzyme, such as an effect of reactive amino
313 acids (His or Cys).

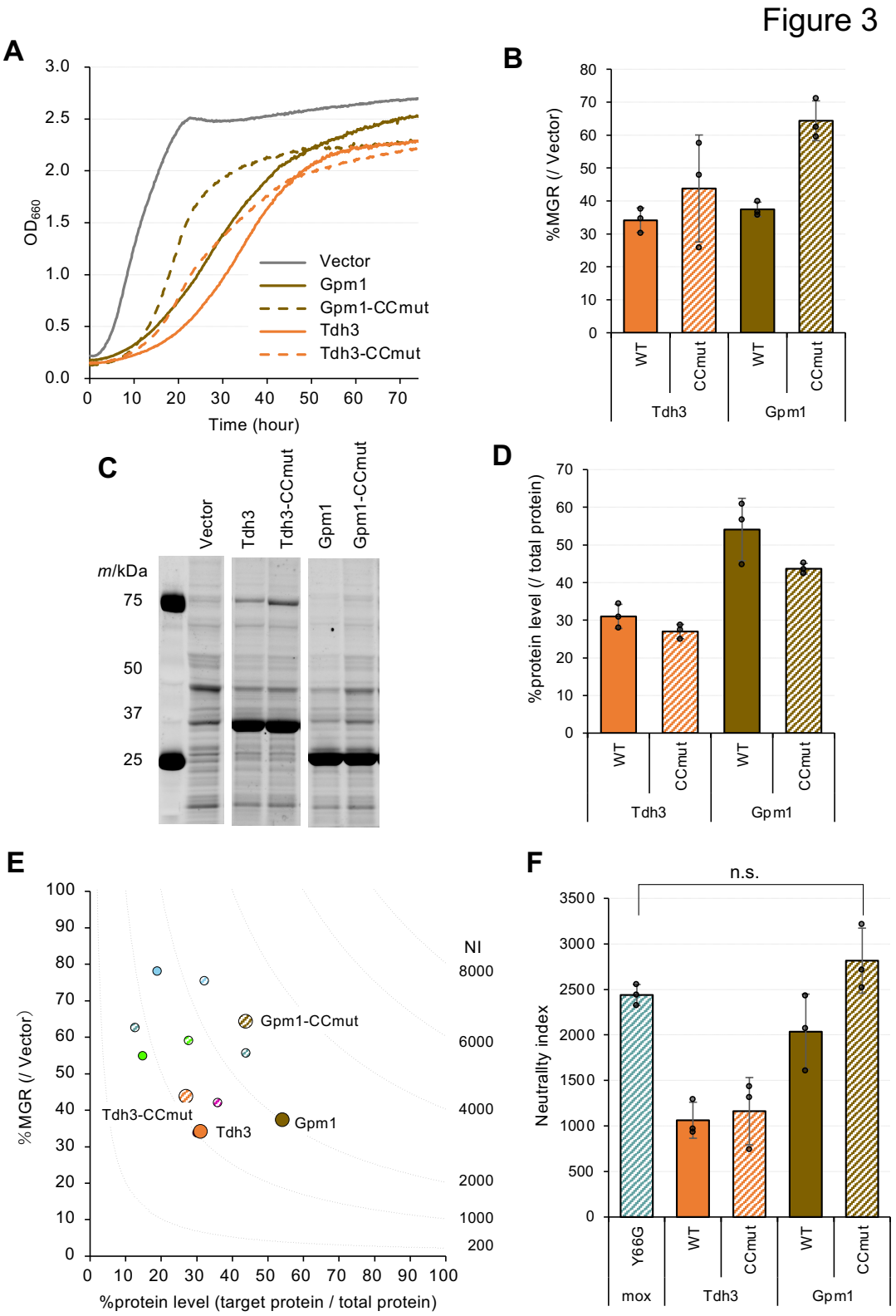

Figure 3. Evaluation of the neutrality of Tdh3 and Gpm1.

A) Growth curves of cells with the control vector (Vector) and overexpressing Gpm1 and Tdp3 and their catalytic center mutants (CCmut) in synthetic medium (–LeuUra). The solid or dotted lines show

318 the average calculated from three biological replicates. Growth curves with SDs of replicates are shown
319 in **Figure S3-S1**.
320 **B**) MGR of cells overexpressing indicated proteins (percent over the vector control).
321 **C**) Gel images of SDS-PAGE-separated proteins extracted from cells overexpressing indicated proteins.
322 All proteins were separated after staining with a fluorescent dye.
323 **D**) Protein levels of the target protein (percent over the total protein). The amount was calculated from
324 the intensity of the target bands separated by SDS-PAGE of **C**.
325 **E**) Relationship between MGR and the protein level. MGR data are the same as in **B**, and the protein
326 level data are the same as in **D**. The neutrality indices (NIs) are indicated by the lines in **Figure 2F**.
327 **F**) The neutrality index for Gpm1, Tdh3, and their CC-mutants.
328 The bars and error bars in **B**, **D**, and **F** show the means and SDs calculated from three biological
329 replicates. The raw data is shown with dot plots.

330
331
332 **Overexpression of mox-YG causes an amino acid starvation response.**
333 To understand the cell physiology under protein burden, we next performed transcriptome (RNA-seq)
334 analysis of the cells overexpressing mox-YG, the least constrained protein. Although the expression
335 limit of mox-YG is about 3-fold higher than that of mox (**Figure 2E**), the growth rates at the expression
336 limits of both are not largely different (**Figure 2C**). Thus, by comparing transcriptomes upon their
337 overexpression, we may be able to distinguish and extract the general transcriptional response due to
338 reduced growth rates from the (protein burden) response associated with the massive expression of a
339 less constrained protein.
340
341 The expression changes under mox and mox-YG overexpression were calculated as fold change (FC)
342 over the vector control (**Figures 4_S1A, B**). The overall trend of expression changes was similar (r =
343 0.64, **Figure 4A**). This similar variation may include responses associated with the expression system
344 and reduced growth rate. On the other hand, there were also different transcriptional responses between
345 the two. Gene categories that showed significant expression changes in either mox or mox-YG

346 overexpression are shown in Figure 4B. In addition to the enhanced ribosome synthesis and decreased
347 glycolysis observed in previous mox overexpression (Namba et al., 2022), enhanced oxidative
348 phosphorylation was detected. Interestingly, "Ribosome biogenesis", which was elevated in mox
349 overexpression, showed a rather decreasing trend in mox-YG overexpression (**Figure 4B**). Indeed,
350 *IFH1*, which is involved in ribosomal gene transcription (Martin et al., 2004), was upregulated in mox,
351 but downregulated in mox-YG (**Figure 4A**). Different trends were also observed for amino acid
352 metabolism (**Figure 4B**). The amino acid transporter genes *AGP1* and *GAP1* were upregulated only in
353 mox-YG overexpression (**Figure 4A**). Expressions of specific amino acid and nitrogen source
354 transporter genes were strongly induced in mox-YG (**Figure 4C**). The expression of glucose transporter
355 genes was also very different (**Figure 4C**). The transcriptional responses in mox-YG overexpression
356 obtained by RNA-seq were confirmed by transcriptional reporter analysis (**Figure 4D, 4_S2**). These
357 results suggest that mox and mox-YG induce similar but distinct transcriptional responses, particularly
358 that mox-YG overexpression may result in depletion of amino acid and nitrogen sources and decreased
359 ribosome synthesis.

Figure 4

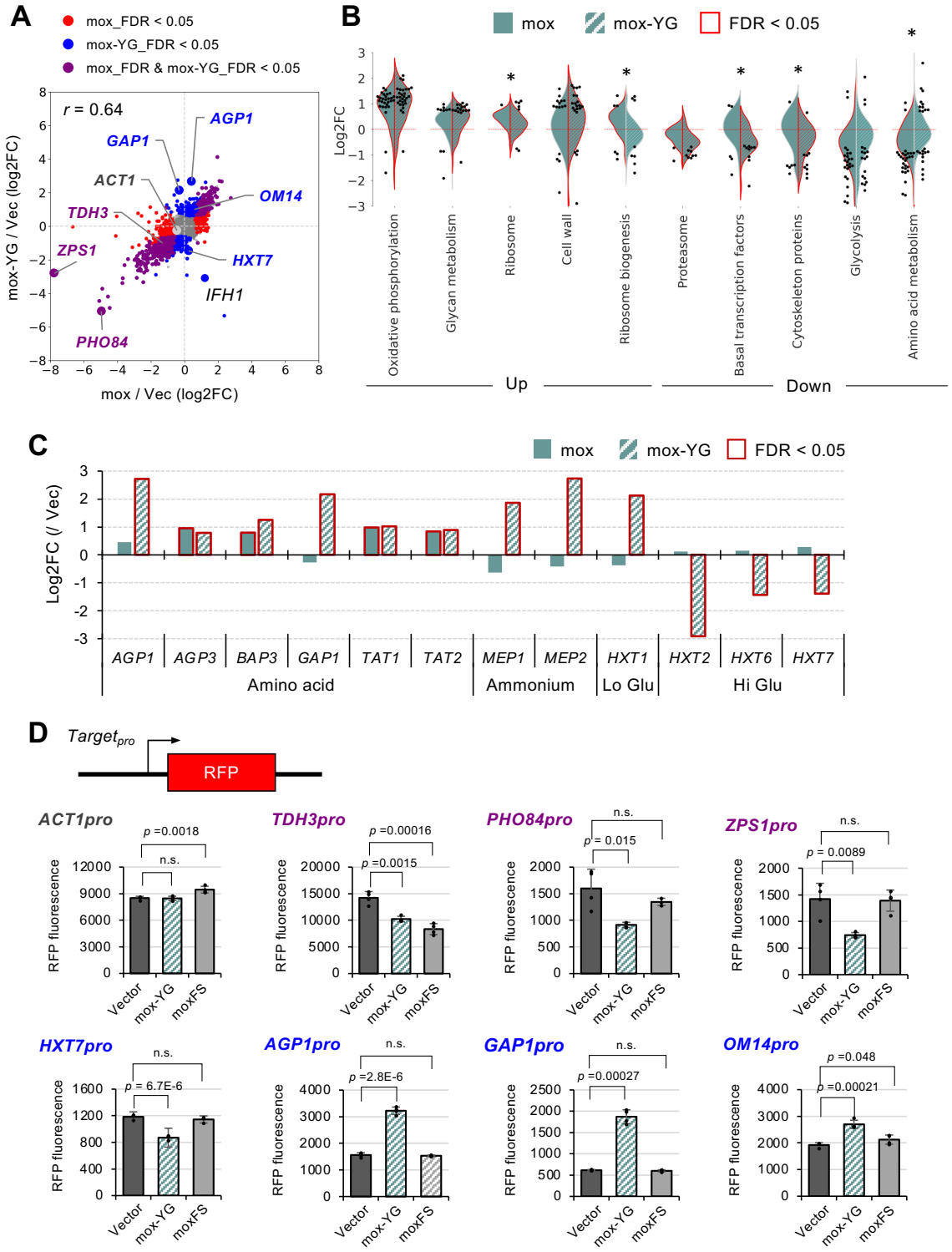

360

361 **Figure 4. Transcriptional response of mox and mox-YG overexpression.**

362 **A)** Comparison of transcriptional responses of mox and mox-YG overexpression. Genes that showed

363 common or different transcriptional responses in mox and mox-YG overexpression are shown in

364 indicated colors. Genes that showed characteristic responses are also shown. FDR: false discovery rate.
365 *r*: Pearson correlation coefficient.
366 **B)** Gene groups that showed significant transcriptional changes. Among the KEGG orthology level 3
367 categories, gene groups in the category that were significantly up-regulated or down-regulated (FDR <
368 0.05) in mox or mox-YG overexpression are shown in the violin plots. Genes with significant expression
369 changes (FDR < 0.05) within the same category are shown by swarm plots. Asterisks indicate significant
370 differences (FDR < 0.05) between mox and mox-YG comparisons in gene groups belonging to the same
371 category. Comparisons for all categories are shown in **Figure 4_S1C**.
372 **C)** Expression changes in representative amino acid, ammonium, and glucose transporters.
373 **D)** Verification of promoter activity by the reporter assay. Constructs used for promoter analysis with
374 transcription reporters and quantitative results of RFP fluorescence values (arbitrary unit) for each
375 promoter. Bars and error bars indicate the mean and SD of maximum fluorescence values for RFP
376 calculated from four biological replicates. Raw data are shown as dot plots. The *p*-values were
377 calculated by performing Welch's *t*-test and applying Bonferroni correction. "n.s." means $p > 0.05$.
378 Detailed constructs and time series data for promoters other than those shown here are in **Figure 4_S2**.
379
380
381 **Overexpression of mox-YG causes a proteomic response that partially overlaps with TORC1**
382 **inactivation.**
383 Protein burden is an overload on synthetic resources, and thus, when this overload occurs strongly, it is
384 expected that there would be a reduction in the amount of proteins other than those being overexpressed
385 due to competition for synthetic resources. Indeed, in cells overexpressing mox-YG, the amounts of
386 proteins other than mox-YG were reduced (**Figure 5A**). Interestingly, the total amount of protein per
387 cell remained almost constant, with the amount of other proteins decreasing as mox-YG was
388 overexpressed. This trend was generally true for the overexpression of other FPs and glycolytic enzymes
389 (**Figure 5_S1**). This suggests that there is a mechanism (or constraint) that maintains the overall cellular
390 protein levels. To examine changes in protein expression, proteomic analysis of mox-YG
391 overexpressing cells was performed. The distribution of intensities obtained from the analysis is shown

392 in the Proteomaps in **Figure 5B**. In mox-YG overexpressing cells, mox-YG accounted for 40% of the
393 total protein expression. **Figure 5A** suggests that in mox-YG overexpressing cells, proteins other than
394 mox-YG are overall reduced to about 60% compared to the vector. Therefore, we considered it
395 necessary to normalize the data overall to accurately represent changes in the per-cell proteome.
396 However, in this study, we used data without such correction to focus on how the composition of the
397 proteome, other than mox-YG, changed (see Materials and Methods and **Figures 5_S2** for more details).
398
399 **Figure 5C** illustrates the categories that showed significant changes upon mox-YG overexpression (all
400 categories are shown in **Figure 5_S3**). Elevated mitochondrial functions, such as oxidative
401 phosphorylation and TCA cycle, and decreased ribosomal protein and ribosomal synthesis were
402 observed. As mentioned above, RNA-seq results suggested nitrogen source starvation in mox-YG
403 overexpression. Therefore, we investigated whether this response is influenced by the regulation
404 through the TORC1 pathway, a primary mechanism responsive to nitrogen sources. By comparing
405 expression changes due to rapamycin (a TORC1 inhibitor) treatment (Gowans et al., 2018) and mox-
406 YG overexpression, we found that about 40% of the proteins with altered expression were congruent
407 with the group of proteins regulated by TORC1 (**Figures 5D, E**). Thus, the proteome expression
408 changes due to mox-YG overexpression may include responses due to inactivation of the TORC1
409 pathway as well as other responses. **Figure 5C** shows which categories had significant expression
410 changes when separated into rapamycin-responsive (Rap) and rapamycin-non-responsive (Non-Rap)
411 gene populations. Carbohydrate metabolism, elevated TCA cycle, and decreased ribosome synthesis
412 were suggested to be responses due to TORC1 inactivation, while endocytosis, cytoskeleton, protein
413 transport and lipid synthesis, and glycolysis were suggested to be due to responses other than TORC1
414 inactivation (**Figure 5_S4**). Oxidative phosphorylation included both Rap responses (12/32) and non-
415 responses (20/32) (**Figure 5_S4C**). We confirmed an increase in Rip1, one of the proteins in the
416 oxidative phosphorylation category, using fluorescence microscopy observations (**Figure 5_S5**). Thus,
417 the massive expression of mox-YG resulted in a decrease in intracellular proteins and changes in
418 proteome composition. The changes included decreased ribosomes and an increase in mitochondrial

419 proteins the primary cause of which seemed to be the inactivation of the TORC1 pathway due to

420 nitrogen source depletion.

Figure 5

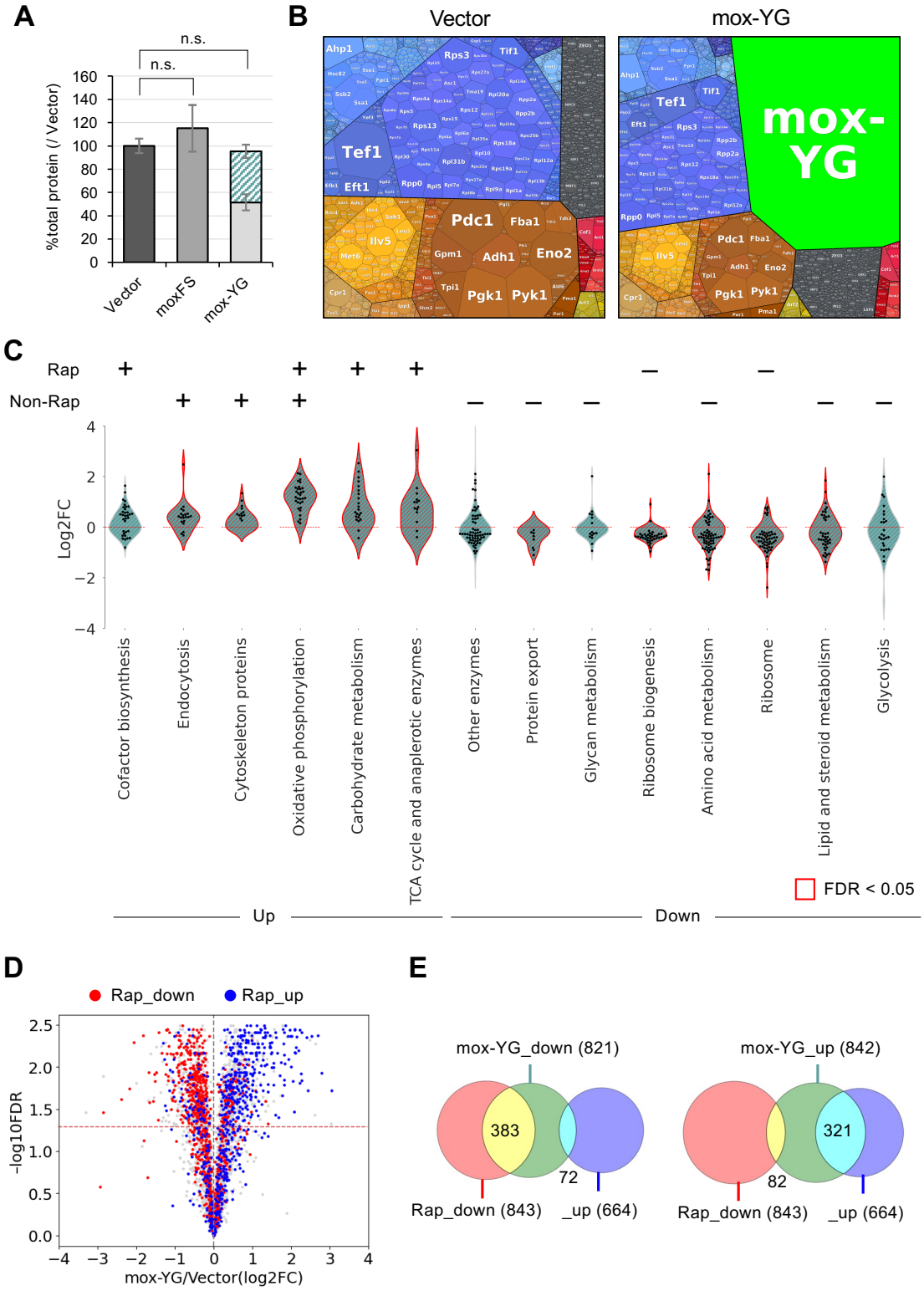

421

422 **Figure 5. Overexpression of mox-YG causes a proteome response like that of TORC1 inactivation.**

423 **A)** Ratio of the total protein amount over the vector. The colored area indicates the amount of
424 overexpressed protein. The amount was calculated from the intensity of the target bands separated by
425 SDS-PAGE. Bars and error bars indicate the mean and SD of protein levels calculated from three
426 biological replicates. The *p*-values were calculated by performing Welch's *t*-test and applying
427 Bonferroni correction. “n.s.” means $p > 0.05$.
428 **B**) Visualization of the proteome of the vector control and mox-YG overexpressing cells using
429 Proteomaps (Liebermeister et al., 2014). Each polygon represents the mass fraction of the protein within
430 the proteome. Similar colors indicate similar or closely related pathways and proteins.
431 **C)** Violin plots showing groups of genes in the KEGG orthology level 3 category whose expression
432 was increased or decreased by mox-YG overexpression. Gene groups with significantly altered
433 expression (FDR < 0.05) in mox-YG overexpression are shown in red. Genes with significant
434 expression changes (FDR < 0.05) within the same category are shown by swarm plots. "+" and "–"
435 indicate the categories with significantly increased or decreased expression, respectively, when
436 separated into Rapamycin-responsive (Rap) and Rapamycin-non-responsive (Non-Rap) gene
437 populations. Comparisons for all categories are shown in **Figures 5_S3 and S4**.
438 **D)** Volcano plots showing genes whose expression levels were altered by rapamycin treatment in the
439 proteome results of mox-YG overexpressing cells.
440 **E)** Venn diagram representing the overlap of the proteome during mox-YG overexpression and
441 rapamycin treatment. The number of genes in each area is shown.
442 For **C**, **D**, and **E**, published data (Gowans et al., 2018) was used for comparison with the rapamycin
443 response genes.
444
445
446 **Overexpression of mox-YG causes a dysplastic nucleolus, which is alleviated by mutations in the**
447 **nuclear exosome.**
448 Ribosomes are a crucial factor for protein burden because they are themselves protein synthesizers
449 while being synthesized in the highest amounts in the cell. Therefore, we further focused on the behavior
450 of ribosomes in mox-YG cells and expression changes were investigated in detail for each ribosomal

451 protein (**Figure 6_S1**). While the majority of the 84 ribosomal proteins detected (45 of them
452 significantly) decreased, six (Rps12, Rps31, Ppp0, Rpp2a, Rpl5, and Rpl12) showed significant
453 increases. Interestingly, all decreased ribosomal proteins are assembled into ribosomes in the nucleolus,
454 while all increased ribosomal proteins are assembled into ribosomes in the cytoplasm (Lafontaine,
455 2015). They constitute the "beak" of the 40S subunit and the "P-stalk" and the "central protuberance
456 (pc)" of the 60S subunit (**Figure 6A**). Electron micrographs showed an abnormal nucleolar formation
457 of mox-YG overexpressing cells (**Figures 6B, 6_S3**), in addition to reduced ribosome density in the
458 cytoplasm (**Figure 6_S2A**). This abnormal nucleolar formation was also confirmed by fluorescence
459 microscopy images of Nsr1 (Nucleolin), the major protein of the nucleolus (**Figure 6_S2B-D**).
460
461 Based on these results, we hypothesized that overexpression of mox-YG creates an imbalance between
462 the amount of ribosomal protein synthesized in the cytoplasm and the amount of rRNA synthesized in
463 the nucleolus (**Figure 6C, D**). The imbalance may lead to the creation of misassembled ribosomes,
464 which are eventually degraded. We speculated that the primary enzyme degrading the misassembled
465 ribosome should be the nuclear exosome. This is because our previous genome-wide mutation analysis
466 identified exosome mutants (*dis3-1, mtr3-ts, mtr4-1, rpn42-ph, rpn45-ph, and ski6-ph*) as primary
467 mitigators of protein burden (Kintaka et al., 2020). We confirmed that the *mtr4-1* mutant does not show
468 growth retardation upon mox-YG overexpression (**Figure 6E**). In fact, in *mtr4-1* cells, there was no
469 difference in growth rate between the vector and mox-YG overexpression (**Figure 6_S5B**), but rather
470 a shorter lag time for the mox-YG overexpression than the vector control (**Figure 6E**). We next
471 quantified protein upon mox-YG overexpression in *mtr4-1* cells (**Figure 6F**). Compared to the wild-
472 type (Vector), the total protein content in *mtr4-1* (Vector) cells was reduced to 78%, which was likely
473 related to the decreased growth. In the *mtr4-1* mox-YG overexpressing cells, the amount of other
474 proteins decreased (to 54%), overwhelmed by the 40% expression of mox-YG. However, the overall
475 protein content increased compared to the *mtr4-1* vector control, with a composition like the wild-type
476 mox-YG overexpressing cells. Therefore, in *mtr4-1* cells, even though mox-YG overexpression reduced
477 the amount of other proteins (to 54%) compared to the vector (78%), the growth rate was not reduced
478 (**Figure 6-S5B**). This suggests that mox-YG overexpression restores the effect of growth inhibition

479 caused by *mtr4-1*. Next, we observed the composition of the nucleolus in *mtr4-1* (**Figures 6G, 6_S6B,**
480 **E**). The failure of nucleolus formation observed upon mox-YG overexpression was partially rescued in
481 the *mtr4-1* strain. This supports our hypothesis that misassembled ribosomes are degraded by the
482 exosome (**Figure 6D**), and with low exosome activity, nucleolus formation (and efficient ribosome
483 assembly) would be possible even with overexpression of mox-YG (**Figure 6_S4D**).
484
485 While experimenting with mox-YG overexpressing cells, we found that these cells stop growth earlier
486 (lower final density) at higher temperatures (38°C) than the vectors (**Figure 6_S6A**). Cells at this time
487 did not show cell death such as cell bursting (**Figure 6_S6**). Recently, it was reported that intracellular
488 osmotic pressure increases at high temperatures, resulting in less formation of liquid-liquid phase-
489 separated structures such as nucleoli, which are recovered when cells are placed in hyperosmotic
490 conditions (Watson et al., 2023). We hypothesized that the growth inhibition of mox-YG
491 overexpressing cells at high temperatures may be due to the enhanced failure of nucleolus formation,
492 and thus cultured mox-YG overexpressing cells under hyperosmotic pressure. At 30°C,
493 hyperosmolarity caused the same decrease in growth for the vector control and mox-YG overexpression
494 (**Figures 6I, 6_S6C**). On the other hand, at 38°C, hyperosmolarity caused a decrease in growth only in
495 the vector control and no further decrease in mox-YG overexpression cells (**Figures 6J, 6_S6D**). The
496 same trend was observed regarding the size of the nucleosome (**Figures 6_S6E, F**). Under the
497 conditions with added sorbitol and under mox-YG overexpression, the size of the nucleoli was
498 smaller than the control at 30°C, whereas, at 38°C, it was rather larger than the control. This
499 suggests that mox-YG overexpression and hyperosmolarity may mitigate each other's growth-inhibitory
500 effects, and one explanation may be that hyperosmolarity suppresses the abnormal organization of the
501 nucleolus caused by mox-YG overexpression.

Figure 6

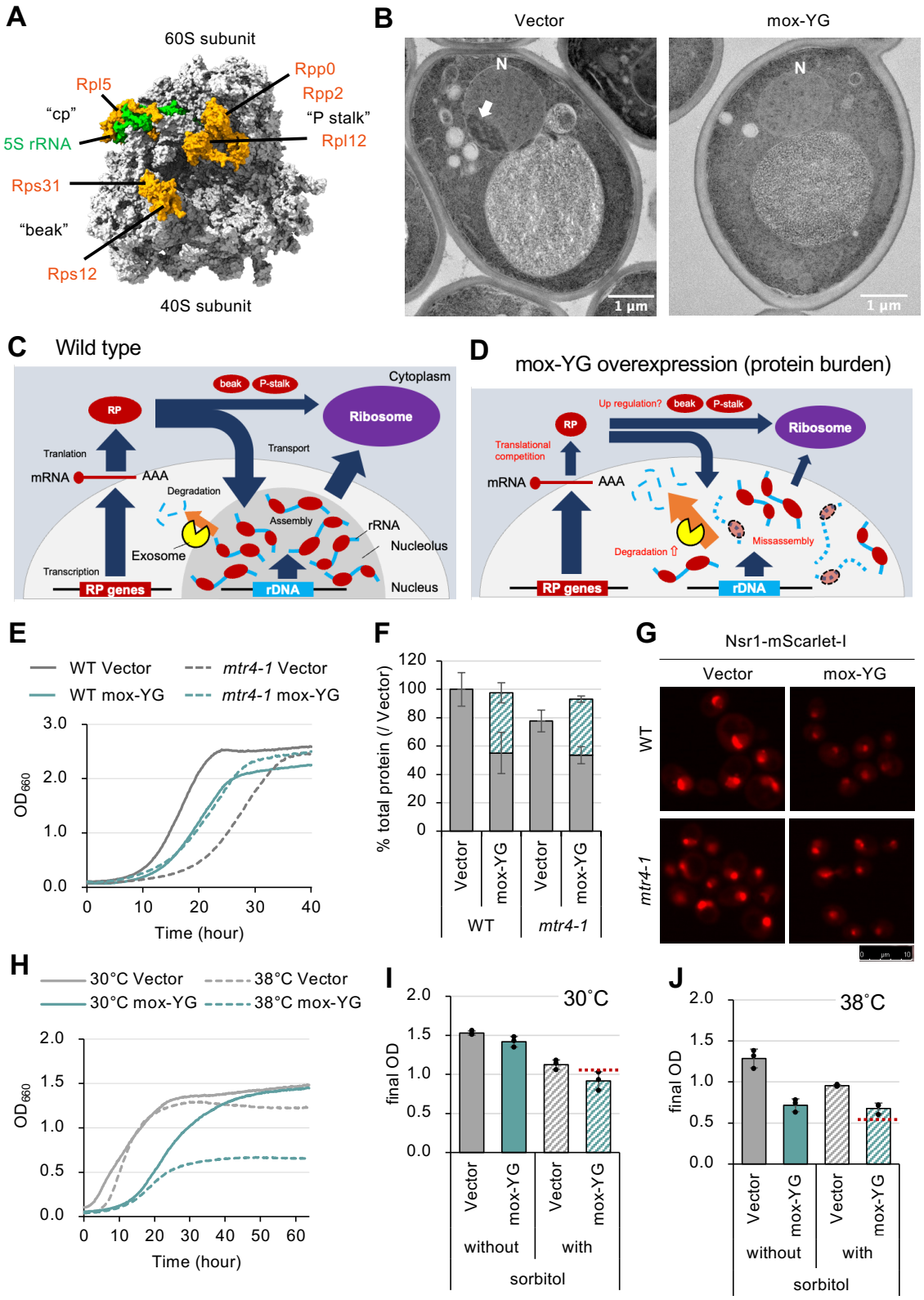

Figure 6. mox-YG overexpression causes abnormal nucleolus formation.

504 **A.** 3D structure of the ribosome. PDB model 6GQV (Pellegrino et al., 2018) is used for the base model
505 and colored using ChimeraX software (Meng et al., 2023). Ribosomal proteins with increased
506 expression upon mox-YG overexpression are shown with the named structures containing them. See
507 also **Figure 6_S1** for the quantitative data.
508 **B)** Electron microscope images of the vector control and mox-YG overexpressing cells. The arrow in
509 the image points to the nucleolus structure. N: nucleus. Images of other observed cells are shown in
510 **Figure S6_S3**.
511 **C, D)** Model diagrams showing the hypothetical situation of the wild type (**C**) and mox-YG
512 overexpressing cells (**D**). In WT cells, enough ribosomal proteins (RPs) are produced, resulting in RP-
513 assembled rRNAs and the formation of nucleolus with normal morphology. On the other hand, in mox-
514 YG overexpressing cells, the amount of RP is reduced due to translation competition, increasing
515 misassembled rRNA. As a result, degradation of rRNA by exosomes may be accelerated, resulting in
516 abnormal nucleolus morphology.
517 **E)** Growth curves of WT and *mtr4-1* mutant cells with the control vector or upon
518 overexpression of mox-YG at 30˚C. The solid or dotted lines show the average calculated from
519 three biological replicates. Growth curves with SDs of replicates are shown in **Figure 6_S5**.
520 **F)** Ratio of total protein levels of WT and *mtr4-1* strains with the vector or upon mox-YG
521 overexpression, calculated the total protein level of WT cells with the control vector as 100%. Gray
522 bars indicate expression levels of proteins other than mox-YG; green shaded bars indicate mox-YG
523 expression levels. Error bars were SDs calculated from three biological replicates.
524 **G)** Fluorescence microscopy image of nucleolus-localized protein Nsr1-mScarlet-I of the WT and *mtr4-*
525 *1* mutant cells with the vector or mox-YG overexpression. Bright field and merged images, and
526 quantification of the nucleolus size are shown in **Figures 6_S5D and S5E**.
527 **H)** Growth curves of the cells with the vector or under mox-YG overexpression cultivated at 30°C or
528 38°C. The solid or dotted lines show the average calculated from three biological replicates. Growth
529 curves with SDs of replicates are shown in **Figure 6_S6A**.

530 **I, J)** Final OD of the cell culture with or without 1M sorbitol at 30°C (**I**) or 38°C (**J**). The bars and error
531 bars show the means and SDs calculated from three biological replicates. The red dotted line indicates
532 the final OD estimated from the product of (mox-YG without sorbitol) / (Vector without sorbitol) and
533 (Vector with sorbitol) / (Vector without sorbitol). Growth curves with SDs of replicates are shown in
534 **Figures 6_S6C, D**.

535 # Discussion

536 In this study, we found that the fluorescent properties of FPs constrain their expression limits. This
537 fluorescence-induced cytotoxicity appears as different phenotypes depending on the FPs; an excess of
538 fluorescent mCherry causes cell enlargement, but such a phenotype was not seen with green fluorescent
539 proteins. On the other hand, the cause of the cytotoxicity is not clear currently. Fluorescence itself does
540 not seem to constrain the expression limit, because the mox expression limit remained the same when
541 cultured in the dark or under strong light (**Figure 2_S6**). We also believe that H_2O_2 generated during
542 fluorophore maturation (Craggs, 2009) is unlikely. In the presence of H_2O_2, mox overexpressing cells
543 grew slightly slower than mox-YG overexpressing cells (**Figure 2_S6B**). However, no transcriptional
544 response to oxidative stress, including the catalase gene (*CTT1*), was seen with mox overexpression
545 (FDR <0.187, over the vector, **Data S1**). Because *CTT1* expression was elevated in mox-YG
546 overexpression (FDR <0.006, over the vector, **Data S1**), presumably due to enhanced respiration, mox-
547 YG overexpression might rather increase oxidative stress tolerance. Conversely, "inactive" proteins
548 might accumulate more without interfering with intracellular functions because both inactive
549 fluorescent proteins and inactive glycolytic enzymes showed higher neutrality (**Figures 2 and 3**).
550 However, our current data did not clarify the mechanism, and investigating more proteins and their
551 variants would be required.
552
553 The currently least cytotoxic proteins, non-fluorescent mox-YG and inactive Gpm1 express more than
554 40% of the total protein, whereas yeast cells can maintain growth under these conditions (**Figures 2**
555 **and 3**). This is higher than the prediction in *E. coli*, which stops growing when 37% of the excess
556 protein is expressed (Bruggeman et al., 2020). This may be due to the very low cytotoxicity of the
557 proteins expressed in this study, or it may be because eukaryotic cells have greater capacity than
558 prokaryotic cells. In the mox-YG overexpressing cells, we observed a previously expected but
559 unobserved cellular physiology of the protein burden: depletion of protein synthesis resources (i.e.,
560 nitrogen source; **Figure 4**) and a decrease in other proteins (glycolytic enzymes and ribosomes; **Figure**
561 **5**), possibly due to competition for synthesis. In addition, metabolic conversion to mitochondria and

562 failure of nucleolus formation were observed (**Figures 5 and 6**). As a matter of fact, the nitrogen source
563 depletion response (**Figure 4**) itself is not self-evident. Because the total protein content in the mox-
564 YG overexpressing cells is the same as that in the vector control (**Figure 5A**), the intracellular nitrogen
565 source used for protein synthesis should not be depleted. Then, why does the nitrogen source depletion
566 response occur? Excess mox-YG may promote wasteful consumption of amino acids and nitrogen, or
567 there may be pathways that sense the amount of "useful proteins" and their ability to be synthesized, or
568 there may be depletion of specific amino acids in mox-YG excess. Another possibility is that there may
569 be some mechanism that maintains the amount of total protein in the cell even when the nitrogen source
570 is depleted. Depletion of nitrogen sources probably results in the inactivation of the TORC1 pathway
571 (**Figure 5C-E**), metabolic conversion from fermentation to respiration, and ribosome depression to an
572 economic mode. In *E. coli*, the ppGpp pathway plays this role (Shachrai et al., 2010). While the above
573 is thought to be a physiological response to protein burden, a defect in ribosome synthesis in the
574 nucleolus was also suggested (**Figure 6B**). This could be due to a conflict between nuclear rRNA
575 synthesis and cytoplasmic protein synthesis or to the negative effects of the inability to create a liquid-
576 liquid phase-separated structure due to dilution effects (see below). The partial restoration of nucleolus
577 formation by a mutation of the exosome (**Figure 6G**) supports this possibility.
578
579 When one type of protein is expressed as much as 40% of the total, as in the present study, the
580 cytoplasmic crowding, viscosity, pH, etc. may change due to the nature of the protein and the effect of
581 the reduced protein by competition. These may alter the movement of substances. It is known that when
582 ribosomes are reduced, the fluidity of large proteins changes (Delarue et al., 2018). Water activity-
583 osmotic pressure may change (Watson et al., 2023), and pH may also be affected. These may affect the
584 formation of liquid-liquid phase-separated structures (Delarue et al., 2018; Watson et al., 2023). The
585 failure of nucleolus formation observed in mox-YG overexpression (**Figure 6B**) may be due to such a
586 condition change. In fact, the growth of mox-YG overexpressing cells is significantly impaired at high
587 temperatures (**Figure 6H**), where liquid-liquid phase separation is less likely to occur (Watson et al.,
588 2023), while the effect appears to be reduced at high osmolarity (**Figure 6J**), where it is more likely to
589 occur (Watson et al., 2023). A mutation of the nuclear exosome restored nucleolus formation (**Figure**

590 **6G**), which might be due to the reformation of the liquid-liquid phase-separated structure (i.e.,
591 nucleolus) by increasing the concentration of rRNA. These have not been considered phenomena that
592 occur with protein overexpression. The engineering of physicochemical properties of the cytoplasm
593 thus may be possible by mass expression of proteins with specific properties.
594
595 In this study, in addition to mox-YG, inactive Gpm1 was also expressed in large amounts as well
596 (**Figure 3**). Both are globular proteins with relatively small molecular weight, but it is not yet clear what
597 characteristics are necessary for them not to be cytotoxic. Further investigation of the neutrality of
598 various proteins will clarify these features. In this study, expression limits were investigated, but no
599 experiments were performed to gradually increase expression levels. For example, it would be
600 meaningful to investigate at what expression level of mox-YG a shift to the economy mode or failure
601 of nucleolus formation occurs. Also, due to the limitations of the experimental system, it may not be
602 possible to express mox-YG to its true limit. The expression of one specific protein cannot be 100% of
603 the total protein, and there is always a limit. As the number of ribosomes continues to decrease due to
604 competition for synthesis, the excess proteins cannot be synthesized either. Thus, there must be a final
605 equilibrium point. A more powerful and controllable expression system would be needed to investigate
606 this. Although the translation system appears to be the primary target of burden in mox-YG
607 overexpression (**Figure 2_S5C, D**), the bottleneck in the expression system may also differ depending
608 on gene design (Hausser et al., 2019).

609 # Materials and Methods

610 **Strains, growth conditions, and yeast transformation**

611 BY4741 (*MATa his3Δ1 leu2Δ0 met15Δ0 ura3Δ0*) (Brachmann et al., 1998) was used as the host strain
612 for the experiments. Yeast culture and transformation were performed as previously described (Amberg
613 et al., 2005). A synthetic complete (SC) medium without uracil (Ura) or leucine (Leu), as indicated,
614 was used for yeast culture. The strains used in the reporter assay are listed in the Key Resource Table.

615

616 **Plasmid construction**

617 The plasmids were constructed by homologous recombination activity of yeast cells (Oldenburg 1997),
618 and their sequences were verified by DNA sequencing. Plasmids used in this study are listed in the Key
619 Resource Table.

620

621 **Genetic tug-of-war**

622 To overexpress a target protein to a level that causes growth inhibition (in this study this is referred to
623 as "expression limit"), we used gTOW (**Figure 2_S1A**) (Moriya et al., 2012, 2006). The gene of the
624 target protein is incorporated into the gTOW plasmid (here, pTOW40836) and introduced into yeast
625 cells lacking *ura3* and *leu2* genes. The selection marker in this case is uracil (–Ura conditions). Since
626 this plasmid has the replication origin of 2 μm plasmid (*2 μ ORI*), this plasmid becomes multicopy in
627 the cell (about 30 in the case of the vector). When yeast cells carrying the plasmid are transferred to a
628 medium without leucine and uracil (–Leu/Ura conditions), the copy number of the plasmid in the cells
629 increases (to about 120 in the case of the vector). This is because *leu2-89* on the plasmid is a *LEU2*
630 allele with a large deletion in its promoter, so cells with higher plasmid copy numbers will grow faster
631 in –Leu/Ura conditions. In other words, *leu2-89* acts as a bias to raise the plasmid copy number in –
632 Leu/Ura conditions. If overexpression of the target protein inhibits growth, the plasmid copy number
633 will be lower than the copy number that gives rise to the critical expression of that protein. In other
634 words, the target gene acts as a bias to lower the plasmid copy number. The resulting tug-of-war

635 between the selection biases created by the two genes leads to a target protein being expressed at close
636 to the critical expression level in –Leu/Ura conditions (the green-colored area in **Figure 2_S1A**).
637
638 **Measuring growth rate**
639 Cellular growth was measured by monitoring OD_{660}, every 10 min using a compact rocking incubator
640 (TVS062CA, ADVANTEC). The max growth rate (MGR) was calculated as described previously
641 (Moriya *et al.* 2006). Average values, SD, and *P*-values of Welch's *t*-test were calculated from at least
642 three biological replicates. The growth data of **Figures 2_S9A**, **2_S9B**, and **4_S2** was measured by
643 monitoring OD_{595}, respectively, every 10 min using a microplate reader (Infinite F200, TECAN).
644
645 **Protein analysis**
646 BY4741 cells overexpressing a target protein were cultivated in SC–Leu/Ura medium. The total protein
647 was extracted from log-phase cells (OD_{660} = 1.0) with a NuPAGE LDS sample buffer (Thermo Fisher
648 Scientific) after 0.2 mol/l NaOH treatment (Kushnirov 2000). For each analysis, the total protein
649 extracted from 1 optical density (OD) unit of cells with OD_{660} was used. For total protein visualization,
650 the extracted total protein was labeled with Ezlabel FluoroNeo (ATTO), as described in the
651 manufacturer's protocol, and separated by 4–12% sodium-dodecyl sulfate acrylamide gel
652 electrophoresis (SDS-PAGE). Proteins were detected and measured using the LAS-4000 image
653 analyzer (GE Healthcare) in SYBR–green fluorescence detection mode and Image Quant TL software
654 (GE Healthcare). Protein quantification was performed as shown in **Figure 2_S1B**. Average values, SD,
655 and *P*-values of Welch's *t*-test were calculated from three biological replicates.
656
657 **Measuring GFP fluorescence**
658 GFP fluorescence (Ex485nm/Em535nm) was measured every 10 min using a microplate reader (Infinite
659 F200, TECAN). Average values, SD, and p-values of Welch's *t*-test were calculated from eight
660 biological replicates.
661

662 **RNA-seq analysis**

663 BY4741 cells overexpressing a target protein were cultured in SC–Leu/Ura medium and harvested at
664 the logarithmic growth phase. RNA extraction was performed according to (Köhrer and Domdey, 1991).
665 The purified RNA was quality checked by BioAnalyzer (Agilent) or MultiNA (Shimazu), and the
666 concentration was measured by Qubit (Thermo Fisher Scientific). Purified RNA was stored at −80°C
667 until subsequent experiments. cDNA libraries were prepared using the TruSeq Stranded Total RNA kit
668 (Illumina), using half the protocol of the TruSeq RNA library prep kit. Three biological replicates were
669 analyzed for all strains. The sequences were checked for read quality by FastP (Chen et al., 2018) and
670 then aligned using Hisat2 (Kim et al., 2019). The aligned data were formatted into bam files by Samtools
671 (Li et al., 2009) and quantified by StringTie (Pertea et al., 2015). Finally, expression level variation
672 analysis was performed by EdgeR (Robinson et al., 2010). The raw data were deposited into DDBJ
673 (accession number: PRJDB18064). The processed data (**Data_S1_RNAseq.csv**) included the average
674 expression levels (log10CPM) of 6685 genes in the vector control, the changes in expression (log2FC)
675 upon overexpression of mox or mox-YG compared to the vector control, and the significance values of
676 expression change (mox_FDR, mox-YG_FDR). **Figures 4_S1A, B** is the visualization of this data using
677 volcano plots. This data is used in subsequent data analyses below.

678

679 **Reporter assay**

680 The strains used for the reporter assay were created by introducing the promoter region of each gene
681 and the sequence of mScarlet-I, a type of RFP, into the *FCY1* locus of the genome as shown in **Figure**
682 **4_S2A**. Correct integration was checked by histidine prototrophy and 5-FC resistance of the strain. The
683 cell density (OD_{595}) and RFP fluorescence (Ex535nm/Em590nm) of the created strains were measured
684 every 10 min using a microplate reader (Infinite F200PRO, TECAN). Average and SD of max RFP
685 fluorescence, and p-values of Welch's *t*-test were calculated from eight biological replicates.

686

687 **Proteome analysis**

688 The vector control and mox-YG overexpressing cells (three biological replicates) were cultured in 5 ml
689 of SC–LeuUra medium with shaking and cells were collected at OD_{660} = 1. Cells were washed twice
690 with PBS, frozen on dry ice, and transported to Kazusa DNA Research Institute. The samples were
691 prepared as described in the previous study (Hughes et al., 2019; Kawashima et al., 2022). The cells
692 were dissolved in 100 mM Tris-HCl (pH 8.0) containing 4% SDS and 20 mM NaCl using BIORUPTOR
693 BR-II (SONIC BIO Co., Kanagawa, Japan). The 20 μg of extracted proteins were quantified using
694 Pierce™ BCA Protein Assay Kit (Thermo Fisher Scientific, WA, USA) at 500 ng/μL. The protein
695 extracts were reduced with 20 mM tris (2-carboxyethyl) phosphine for 10 min at 80 °C followed by
696 alkylation with 30 mM iodoacetamide for 30 min at room temperature in the dark. Protein purification
697 and digestion were performed using the sample preparation (SP3) method (Kawashima et al., 2022).
698 The tryptic digestion was performed using 500 ng/μL Trypsin/Lys-C Mix (Promega, Madison, WI,
699 USA) for overnight at 37 °C. The digests were purified using GL-Tip SDB (GL Sciences, Tokyo, Japan)
700 according to the manufacturer's protocol. The peptides were dissolved again in 2% ACN containing
701 0.1% TFA and quantified using BCA assay at 150 ng/μL. The digested peptides were loaded directly
702 using a 75 μm × 12 cm nanoLC nano-capillary column (Nikkyo Technos Co., Ltd., Tokyo, Japan) at
703 40°C and then separated with a 30-minute gradient (mobile phase A = 0.1% FA in water, B = 0.1% FA
704 in 80% ACN) consisting of 0 min 8% B, 30 min 70% B at a flow rate of 200 nL/min using an UltiMate
705 3000 RSLCnano LC system (Thermo Fisher Scientific). The eluted peptides were detected using a
706 quadrupole Orbitrap Exploris 480 hybrid mass spectrometer (Thermo Fisher Scientific) with normal
707 window DIA. The MS1 scan range was set as a full scan with m/z 490-745 at a mass resolution of
708 15,000 to set an Auto Gain Control (AGC) target for MS1 as 3×10^6 and a maximum injection time of
709 23 msec. The MS2 were collected at more than m/z 200 at 30,000 resolutions to set an AGC target of 3
710 $\times 10^6$, maximum injection time of "auto", and fixed normalized collision energy of 28%. The isolation
711 width for MS2 was set to 4 m/z, and for the 500-740 m/z window pattern, an optimized window
712 arrangement was used in Scaffold DIA (Proteome Software, Inc., Portland, OR, USA). The raw data
713 were searched against an *in silico* predicted spectral library using DIA-NN (Demichev et al., 2020).
714 (version:1.8.1, https://github.com/vdemichev/DiaNN) First, an *in-silico* predicted spectral library was
715 generated from the human protein sequence database (UniProt id UP000005640, reviewed, canonical,

716 20381 entries) using DIA-NN. The DIA-NN search parameters were as follows: protease, trypsin;
717 missed cleavages, 1; peptide length range, 7-45; precursor charge range, 2-4; precursor mass range,
718 495-745; fragment ion m/z range, 200-1800; mass accuracy, 10 ppm; static modification, cysteine
719 carbamidomethylation; enabled "Heuristic protein interferences," "Use isotopologues," "MBR," and
720 "No shared spectra." Additional commands were set as follows: "mass acc cal 10," "peak translation,"
721 and "matrix spec q". The protein identification threshold was set at < 1% for both peptide and protein
722 false discovery rates (FDRs). The signal intensity data for 4241 proteins (Data_S2_Proteome.csv) was
723 used for further data analysis below.
724
725 **Data analysis**
726 The analysis and visualization of RNAseq data and proteome data were conducted using
727 custom Python code, and coding and execution were carried out in the Collaboratory. In the
728 RNAseq data, 6,685 protein-coding genes were detected (Data_S1_RNAseq.csv). Among
729 these, 4,291 genes assigned to various categories of KEGG Orthology level 3 (Kanehisa et al.,
730 2023) were placed into 77 categories. Analysis was performed on 47 categories that contained
731 more than 10 gene elements. We investigated whether the expression of genes in each category,
732 as a group, was significantly higher or lower upon overexpression of mox and mox-YG
733 compared to the vector. Specifically, mox/vector (log2FC) and mox-YG/vector (log2FC) were
734 calculated along with their FDR values, and each gene was assigned to a KEGG orthology level
735 3 category. Next, whether the gene groups within each category showed significantly higher or
736 lower expression changes compared to gene groups outside of their category was tested using
737 the Mann-Whitney U test. Significant differences were indicated in the graphs with a red border
738 and red stripes. The graphs showed the overall distribution of genes within each category using
739 violin plots, and only genes showing significant differences in mox/vector (log2FC) and mox-
740 YG/vector (log2FC) were highlighted in swarm plots. An asterisk indicated significant
741 differences on the graphs when the expression changes (log2FC) between mox/vector and mox-

742 YG/vector were significant by the Mann-Whitney U test. The significance threshold was set at
743 FDR < 0.05 for all. Only categories where either mox or mox-YG overexpression showed
744 significant expression changes were extracted and presented as **Figure 4B**, and all 47 categories
745 were shown in **Figure 4_S1**.

746 The proteome analysis was conducted using the signal intensity data (**Data_S2_proteome.csv**).
747 This data includes proteins that were detected only in some samples under certain conditions
748 or replicates, especially those with low signals or large expression variations. Additionally, the
749 total protein signal sum excluding mox-YG was almost the same between the vector control
750 and mox-YG overexpression (**Figure 5_S2A**). This result contradicts the SDS−PAGE findings,
751 which indicate that the total protein mass per cell, including mox-YG, is the same between the vector
752 control and mox-YG overexpression (**Figure 5A**). Therefore, it is considered necessary to adjust
753 the total protein signal sum, including mox-YG, to match that of the vector control to
754 understand the proteome change per cell. In this study, however, we used the most conservative
755 approach by removing proteins with zero values and not applying any overall corrections
756 (**Figure 5_S2B**), which allowed the analysis of 3,588 proteins. Although this may not correctly
757 analyze "per cell" proteome change, it enables us to capture the change in proteome
758 composition (excluding mox-YG), thus providing information about cellular responses. If the
759 total correction is applied, only 138 proteins were increased (**Figure 5_S2B**), most of which
760 are mitochondrial proteins.

761 For the detected 3,588 proteins above, we compared the increase or decrease of protein groups
762 within each category of KEGG Orthology Level 3 with those outside the category. Analysis
763 was performed on 45 categories, each containing more than 10 proteins, to investigate whether
764 the expression of protein groups in each category was significantly higher or lower under mox-
765 YG overexpression compared to the vector control. Specifically, the average log2FC and its

766 FDR values were calculated using data from three replicates for mox-YG/vector, and each
767 protein was assigned to a KEGG orthology level 3 category. Next, whether the protein groups
768 within each category showed significantly higher or lower expression changes compared to
769 protein groups outside of their category was tested using the Mann-Whitney U test. Significant
770 differences were indicated in the graphs with a red border and red stripes. The graphs showed
771 the overall distribution of proteins within each category using violin plots, and only proteins
772 showing significant differences in mox-YG/vector (log2FC) were highlighted in swarm plots.
773 The significance threshold was set at FDR < 0.05 for all. Only categories where mox-YG
774 overexpression showed significant expression changes were extracted and presented in **Figure**
775 **5C** and all 47 categories were shown in **Figure 5_S3**. Published data (Gowans et al., 2018) was
776 used to separate protein groups into rapamycin-responsive and non-responsive, and similar
777 analysis and visualization were conducted (**Figures 5_S4A, B**).

778

779 **Fluorescence microscopic observation**

780 Cells overexpressing target proteins were cultured in SC-LeuUra medium and observed under an
781 inverted microscope (DMI 6000 B, Leica) at log phase (OD660 = 1.0). Images were acquired with Leica
782 Application Suite and processed with Leica Application Suite X software (Leica Microsystems). Cells
783 in brightfield images were separated from the images using yeast_segmentation-master_v3 (Lu et al.,
784 2019). Cell morphological traits were assessed using parameters obtained when analysed using
785 CellProfiler (Ver. 4.2.6) (Carpenter et al., 2006). "AreaShape_Area" was used to analyse FP-
786 overexpressing cell size in **Figure 2_S5B**, Nsr1-GFP in **Figure 6_S2C** and Nsr1-mScarlet-I in **Figure**
787 **6_S5E, S6**F. For analysis of the fluorescence intensity of Rip1-mScarlet-I in **Figure 5_S5B**,
788 "Intensity_IntegratedIntensity" was used. Intensity_MeanIntensity" was used to analyze the
789 fluorescence intensity of Nsr1-GFP in **Figure 6_S2D**. Ten images per experiment were used for analysis.

790

791 **Electron microscopic observation**

792 Cells grown to log phase (OD_{600} = 1.0) at 30°C in SC–LeuUra medium were collected and transported
793 to Tokai Electron Microscope Co. Transported samples were sandwiched between copper plates, flash-
794 frozen with liquefied propane, and then dehydrated with anhydrous ethanol. cells were fixed with a 5:5
795 mixture of propylene oxide and resin (Quetol-651, Nissin EM Co.). Fixed cells were cut with an
796 ultramicrotome (Ultracut UCT, Leica) to prepare 80 nm thick sections, stained with 2% uranyl acetate
797 and lead stain solution (Sigma-Aldrich Co.), and observed with a transmission electron microscope
798 (JEM-1400 Plus, JEOL Ltd.).

Acknowledgments

We thank the members of the Moriya laboratory (Okayama University) for their helpful discussions. This work was partly supported by JSPS KAKENHI Grant Numbers 18H04824 20H03242, and 20H04870.

803 # References

804 Amberg DC, Burke DJ, Burke D, Strathern JN. 2005. Methods in Yeast Genetics: A Cold Spring
805 Harbor Laboratory Course Manual. CSHL Press.

806 Bolognesi B, Lorenzo Gotor N, Dhar R, Cirillo D, Baldrighi M, Tartaglia GG, Lehner B. 2016. A
807 Concentration-Dependent Liquid Phase Separation Can Cause Toxicity upon Increased Protein
808 Expression. *Cell Rep* **16**:222–231.

809 Brachmann CB, Davies A, Cost GJ, Caputo E, Li J, Hieter P, Boeke JD. 1998. Designer deletion
810 strains derived from Saccharomyces cerevisiae S288C: a useful set of strains and plasmids for
811 PCR-mediated gene disruption and other applications. *Yeast* **14**:115–132.

812 Bruggeman FJ, Planqué R, Molenaar D, Teusink B. 2020. Searching for principles of microbial
813 physiology. *FEMS Microbiol Rev* **44**:821–844.

814 Carpenter AE, Jones TR, Lamprecht MR, Clarke C, Kang IH, Friman O, Guertin DA, Chang JH,
815 Lindquist RA, Moffat J, Golland P, Sabatini DM. 2006. CellProfiler: image analysis software for
816 identifying and quantifying cell phenotypes. *Genome Biol* **7**:R100.

817 Chen S, Zhou Y, Chen Y, Gu J. 2018. fastp: an ultra-fast all-in-one FASTQ preprocessor.
818 *Bioinformatics* **34**:i884–i890.

819 Costantini LM, Baloban M, Markwardt ML, Rizzo M, Guo F, Verkhusha VV, Snapp EL. 2015. A
820 palette of fluorescent proteins optimized for diverse cellular environments. *Nat Commun* **6**:7670.

821 Craggs TD. 2009. Green fluorescent protein: structure, folding and chromophore maturation. *Chem*
822 *Soc Rev* **38**:2865–2875.

823 Delarue M, Brittingham GP, Pfeffer S, Surovtsev IV, Pinglay S, Kennedy KJ, Schaffer M, Gutierrez
824 JI, Sang D, Poterewicz G, Chung JK, Plitzko JM, Groves JT, Jacobs-Wagner C, Engel BD, Holt
825 LJ. 2018. mTORC1 Controls Phase Separation and the Biophysical Properties of the Cytoplasm
826 by Tuning Crowding. *Cell* **174**:338–349.e20.

827 Demichev V, Messner CB, Vernardis SI, Lilley KS, Ralser M. 2020. DIA-NN: neural networks and
828 interference correction enable deep proteome coverage in high throughput. *Nat Methods* **17**:41–
829 44.

830 Dong H, Nilsson L, Kurland CG. 1995. Gratuitous overexpression of genes in Escherichia coli leads
831 to growth inhibition and ribosome destruction. *J Bacteriol* **177**:1497–1504.
832 Eguchi Y, Makanae K, Hasunuma T, Ishibashi Y, Kito K, Moriya H. 2018. Estimating the protein
833 burden limit of yeast cells by measuring the expression limits of glycolytic proteins. *Elife* **7**.
834 doi:10.7554/eLife.34595
835 Farkas Z, Kalapis D, Bódi Z, Szamecz B, Daraba A, Almási K, Kovács K, Boross G, Pál F, Horváth
836 P, Balassa T, Molnár C, Pettkó-Szandtner A, Klement É, Rutkai E, Szvetnik A, Papp B, Pál C.
837 2018. Hsp70-associated chaperones have a critical role in buffering protein production costs.
838 *Elife* **7**. doi:10.7554/eLife.29845
839 Frumkin I, Schirman D, Rotman A, Li F, Zahavi L, Mordret E, Asraf O, Wu S, Levy SF, Pilpel Y.
840 2017. Gene Architectures that Minimize Cost of Gene Expression. *Mol Cell* **65**:142–153.
841 Gowans GJ, Schep AN, Wong KM, King DA, Greenleaf WJ, Morrison AJ. 2018. INO80 Chromatin
842 Remodeling Coordinates Metabolic Homeostasis with Cell Division. *Cell Rep* **22**:611–623.
843 Hausser J, Mayo A, Keren L, Alon U. 2019. Central dogma rates and the trade-off between precision
844 and economy in gene expression. *Nat Commun* **10**:68.
845 Hughes CS, Moggridge S, Müller T, Sorensen PH, Morin GB, Krijgsveld J. 2019. Single-pot, solid-
846 phase-enhanced sample preparation for proteomics experiments. *Nat Protoc* **14**:68–85.
847 Kafri M, Metzl-Raz E, Jona G, Barkai N. 2016. The Cost of Protein Production. *Cell Rep* **14**:22–31.
848 Kaizu K, Moriya H, Kitano H. 2010. Fragilities caused by dosage imbalance in regulation of the
849 budding yeast cell cycle. *PLoS Genet* **6**:e1000919.
850 Kanehisa M, Furumichi M, Sato Y, Kawashima M, Ishiguro-Watanabe M. 2023. KEGG for
851 taxonomy-based analysis of pathways and genomes. *Nucleic Acids Res* **51**:D587–D592.
852 Kastberg LLB, Ard R, Jensen MK, Workman CT. 2022. Burden Imposed by Heterologous Protein
853 Production in Two Major Industrial Yeast Cell Factories: Identifying Sources and Mitigation
854 Strategies. *Front Fungal Biol* **3**:827704.
855 Kawashima Y, Nagai H, Konno R, Ishikawa M, Nakajima D, Sato H, Nakamura R, Furuyashiki T,
856 Ohara O. 2022. Single-Shot 10K Proteome Approach: Over 10,000 Protein Identifications by
857 Data-Independent Acquisition-Based Single-Shot Proteomics with Ion Mobility Spectrometry. *J*

858 *Proteome Res* **21**:1418–1427.

859 Keppler-Ross S, Noffz C, Dean N. 2008. A new purple fluorescent color marker for genetic studies in
860 Saccharomyces cerevisiae and Candida albicans. *Genetics* **179**:705–710.

861 Keren L, Hausser J, Lotan-Pompan M, Vainberg Slutskin I, Alisar H, Kaminski S, Weinberger A,
862 Alon U, Milo R, Segal E. 2016. Massively Parallel Interrogation of the Effects of Gene
863 Expression Levels on Fitness. *Cell* **166**:1282–1294.e18.

864 Kim D, Paggi JM, Park C, Bennett C, Salzberg SL. 2019. Graph-based genome alignment and
865 genotyping with HISAT2 and HISAT-genotype. *Nat Biotechnol* **37**:907–915.

866 Kintaka R, Makanae K, Moriya H. 2016. Cellular growth defects triggered by an overload of protein
867 localization processes. *Scientific Reports*. doi:10.1038/srep31774

868 Kintaka R, Makanae K, Namba S, Kato H, Kito K, Ohnuki S, Ohya Y, Andrews BJ, Boone C, Moriya
869 H. 2020. Genetic profiling of protein burden and nuclear export overload. *Elife* **9**.
870 doi:10.7554/eLife.54080

871 Koch AL. 1983. The protein burden oflac operon products. *J Mol Evol* **19**:455–462.

872 Köhrer K, Domdey H. 1991. [27] Preparation of high molecular weight RNAMethods in
873 Enzymology. Academic Press. pp. 398–405.

874 Kummer AD, Wiehler J, Rehaber H, Kompa C, Steipe B, Michel-Beyerle ME. 2000. Effects of
875 Threonine 203 Replacements on Excited-State Dynamics and Fluorescence Properties of the
876 Green Fluorescent Protein (GFP). *J Phys Chem B* **104**:4791–4798.

877 Lafontaine DLJ. 2015. Noncoding RNAs in eukaryotic ribosome biogenesis and function. *Nat Struct*
878 *Mol Biol* **22**:11–19.

879 Liebermeister W, Noor E, Flamholz A, Davidi D, Bernhardt J, Milo R. 2014. Visual account of
880 protein investment in cellular functions. *Proc Natl Acad Sci U S A* **111**:8488–8493.

881 Li H, Handsaker B, Wysoker A, Fennell T, Ruan J, Homer N, Marth G, Abecasis G, Durbin R, 1000
882 Genome Project Data Processing Subgroup. 2009. The Sequence Alignment/Map format and
883 SAMtools. *Bioinformatics* **25**:2078–2079.

884 Lu AX, Zarin T, Hsu IS, Moses AM. 2019. YeastSpotter: accurate and parameter-free web
885 segmentation for microscopy images of yeast cells. *Bioinformatics* **35**:4525–4527.

886 Mahima, Sharma AK. 2023. Optimization of ribosome utilization in Saccharomyces cerevisiae. *PNAS*
887 *Nexus* **2**:gad074.
888 Makanae K, Kintaka R, Makino T, Kitano H, Moriya H. 2013. Identification of dosage-sensitive
889 genes in Saccharomyces cerevisiae using the genetic tug-of-war method. *Genome Res* **23**:300–
890 311.
891 Ma L, Pang CNI, Li SS, Wilkins MR. 2010. Proteins Deleterious on Overexpression Are Associated
892 with High Intrinsic Disorder, Specific Interaction Domains, and Low Abundance. *J Proteome*
893 *Res* **9**:1218–1225.
894 Martin DE, Soulard A, Hall MN. 2004. TOR regulates ribosomal protein gene expression via PKA
895 and the Forkhead transcription factor FHL1. *Cell* **119**:969–979.
896 Meng EC, Goddard TD, Pettersen EF, Couch GS, Pearson ZJ, Morris JH, Ferrin TE. 2023. UCSF
897 ChimeraX: Tools for structure building and analysis. *Protein Sci* **32**:e4792.
898 Metzl-Raz E, Kafri M, Yaakov G, Barkai N. 2020. Gene Transcription as a Limiting Factor in Protein
899 Production and Cell Growth. *G3* **10**:3229–3242.
900 Metzl-Raz E, Kafri M, Yaakov G, Soifer I, Gurvich Y, Barkai N. 2017. Principles of cellular resource
901 allocation revealed by condition-dependent proteome profiling. *Elife* **6**. doi:10.7554/eLife.28034
902 Moriya H. 2015. Quantitative nature of overexpression experiments. *Mol Biol Cell* **26**:3932–3939.
903 Moriya H, Makanae K, Watanabe K, Chino A, Shimizu-Yoshida Y. 2012. Robustness analysis of
904 cellular systems using the genetic tug-of-war method. *Mol Biosyst* **8**:2513–2522.
905 Moriya H, Shimizu-Yoshida Y, Kitano H. 2006. In vivo robustness analysis of cell division cycle
906 genes in Saccharomyces cerevisiae. *PLoS Genet* **2**:e111.
907 Namba S, Kato H, Shigenobu S, Makino T, Moriya H. 2022. Massive expression of cysteine-
908 containing proteins causes abnormal elongation of yeast cells by perturbing the proteasome. *G3*
909 **12**. doi:10.1093/g3journal/jkac106
910 Papp B, Pál C, Hurst LD. 2003. Dosage sensitivity and the evolution of gene families in yeast. *Nature*
911 **424**:194–197.
912 Pellegrino S, Demeshkina N, Mancera-Martinez E, Melnikov S, Simonetti A, Myasnikov A, Yusupov
913 M, Yusupova G, Hashem Y. 2018. Structural Insights into the Role of Diphthamide on

914 Elongation Factor 2 in mRNA Reading-Frame Maintenance. *J Mol Biol* **430**:2677–2687.
915 Pertea M, Pertea GM, Antonescu CM, Chang T-C, Mendell JT, Salzberg SL. 2015. StringTie enables
916 improved reconstruction of a transcriptome from RNA-seq reads. *Nat Biotechnol* **33**:290–295.
917 Prelich G. 2012. Gene overexpression: uses, mechanisms, and interpretation. *Genetics* **190**:841–854.
918 Robinson MD, McCarthy DJ, Smyth GK. 2010. edgeR: a Bioconductor package for differential
919 expression analysis of digital gene expression data. *Bioinformatics* **26**:139–140.
920 Scott M, Gunderson CW, Mateescu EM, Zhang Z, Hwa T. 2010. Interdependence of cell growth and
921 gene expression: origins and consequences. *Science* **330**:1099–1102.
922 Shachrai I, Zaslaver A, Alon U, Dekel E. 2010. Cost of unneeded proteins in E. coli is reduced after
923 several generations in exponential growth. *Mol Cell* **38**:758–767.
924 Stoebel DM, Dean AM, Dykhuizen DE. 2008. The cost of expression of Escherichia coli lac operon
925 proteins is in the process, not in the products. *Genetics* **178**:1653–1660.
926 Vavouri T, Semple JI, Garcia-Verdugo R, Lehner B. 2009. Intrinsic protein disorder and interaction
927 promiscuity are widely associated with dosage sensitivity. *Cell* **138**:198–208.
928 Watson JL, Seinkmane E, Styles CT, Mihut A, Krüger LK, McNally KE, Planelles-Herrero VJ,
929 Dudek M, McCall PM, Barbiero S, Vanden Oever M, Peak-Chew SY, Porebski BT, Zeng A,
930 Rzechorzek NM, Wong DCS, Beale AD, Stangherlin A, Riggi M, Iwasa J, Morf J, Miliotis C,
931 Guna A, Inglis AJ, Brugués J, Voorhees RM, Chambers JE, Meng Q-J, O'Neill JS, Edgar RS,
932 Derivery E. 2023. Macromolecular condensation buffers intracellular water potential. *Nature*
933 **623**:842–852.
934 Youn J-Y, Friesen H, Nguyen Ba AN, Liang W, Messier V, Cox MJ, Moses AM, Andrews B. 2017.
935 Functional Analysis of Kinases and Transcription Factors in Saccharomyces cerevisiae Using an
936 Integrated Overexpression Library. *G3* **7**:911–921.